Available online at www.sciencedirect.com
SCIENCE DIRECT®
Surface Science 542 (2003) 94–100
SURFACE SCIENCE
www.elsevier.com/locate/susc

Scanning tunneling microscopy study of superlattice domain boundaries on graphite surface

Hai-Lin Sun *, Quan-Tong Shen, Jin-Feng Jia, Qing-Zhe Zhang, Qi-Kun Xue *

State Key Laboratory for Surface Physics and International Center for Quantum Structures, Institute of Physics, Chinese Academy of Sciences, Beijing 100080, China

Received 3 October 2002; accepted for publication 3 July 2003

Abstract

Domain boundaries of superlattices formed on the highly oriented pyrolytic graphite surface are studied by scanning tunneling microscopy. Twist and glide boundaries are identified with help of theoretical simulations. The apparent vertical corrugation difference of the superlattices with the same lattice periodicity is explained in terms of overlayer attenuation. Our study reveals that the intra-layer strain has important effect on the electronic structure of the graphite surface.

Keywords: Superlattices; Scanning tunneling microscopy; Graphite

1. Introduction

Since the invention of scanning tunneling microscope (STM), highly oriented pyrolytic graphite (HOPG) has become a popular substrate for many purposes of research due to its flat cleavage surface and chemical inertness. "Atomic resolution" can be easily obtained by STM even in air ambient condition. HOPG consists of layers of sp^2 carbon atoms [1], and the layers are weakly bonded together by van der Waals (VDW) force with an ABAB stacking sequence along the c axis. Its electronic properties near the Fermi level are determined by delocalized π states. Two most notable features of the graphite surface, as observed by STM, are the three-fold (rather than six-fold) symmetry [2] and large vertical corrugation amplitude [3]. The ABAB stacking sequence gives rise to two inequivalent atomic sites in a surface unit cell: the α-site carbon atom lies directly above the second-layer atom, whereas the β-site carbon atom is located above the center (the hollow site) of the six-fold carbon ring in the second layer. The interlayer interaction creates a band overlap and moves wave functions of the α atoms away from the Fermi energy. Therefore, only the β-sites atoms are visible to STM, which explains the three-fold symmetry of the STM images. The origin of the anomalous large corrugation is not fully understood and may be related to both physical and electronic effects.

* Corresponding authors. Tel.: +86-108-264-9561; fax: +86-108-264-9228.
E-mail addresses: shlin@aphy.iphy.ac.cn (H.-L. Sun), qkxue@aphy.iphy.ac.cn (Q.-K. Xue).

0039-6028/$ - see front matter © 2003 Elsevier B.V. All rights reserved.
doi:10.1016/S0039-6028(03)00949-X

There are a lot of intrinsic defects on the cleaved graphite surface, such as graphite strand, fiber, ridge, folded-over flake and pieces and broken carbon particles [4,5]. When using HOPG as a conducting substrate to study biological/organic molecules and nanotubes and nanowires, as the sizes and shapes of these defects vary dramatically, one has to be very careful about the image interpretation.

Another prominent intrinsic feature [3,6–17] often observed by STM is superlattice, which has been generally interpreted as a moiré pattern originating from a rotation between the top and underlying graphite layers. The periodicities of the moiré pattern are usually several to tens of nanometers and the corrugation is among several angstroms. The large corrugation in the STM images is not due to physical buckling, but to electronic properties associated with different stacking sequences [3,8,9]. However, a commonly accepted agreement on the origin of this superstructure has not achieved yet. Garbarz et al. [7] attribute the superlattice network to an array of basal dislocations, although further studies by Beyer et al. [16] do not support it. Bernhardt et al. [11] find that superlattice constants in the strained area vary continuously, and the intralayer strain could play an important role in the formation of the superlattice. Based on a theoretical consideration, Kobayashi [18] points out that the nanoscale waves could propagate through many layers without decay due to typical value of the Fermi energies, which is supported by an STM study by Ousing et al. [12]. An agreement on the origin of the superlattice has not been achieved yet.

In this paper, we report on an STM study of the domain boundaries appeared on the graphite surface superlattice. We will show that one graphite layer can significantly decrease the apparent vertical height of a moiré pattern, and it is unlikely that a moiré contrast several layers below can be detected by STM. Based on a good agreement between our experiment and simulation, layer twisting and gliding are proposed to explain the observed domain boundaries. We will also discuss the effect of intra-layer strain on the electronic structure of the superlattices.

2. Experimental

Clean HOPG surface is prepared by common cleaving procedure. The experiments are carried out in a commercial scanning tunneling microscopy system (Park Scientific Instrument, VP). Chemical etched tungsten tips are used as the STM probe. The samples are slightly annealed in ultrahigh vacuum chamber (base pressure 10^{-9} Torr) to get rid of the adsorbed water and contaminants on the surface. Atomic resolution STM images of the graphite surface can routinely be achieved, and the graphite lattice and steps are used to calibrate our STM.

3. Results and discussion

Fig. 1 shows an STM image of the superlattice formed on the cleaved HOPG surface. Two domains with different apparent vertical corrugations are marked by X and Y, respectively. A string of bead-like bright spots forms the boundaries of the superlattice, which are almost the same as that reported previously for the moiré pattern on HOPG [8,11]. A closer view of the boundary between the X and Y domains, as zoomed from the

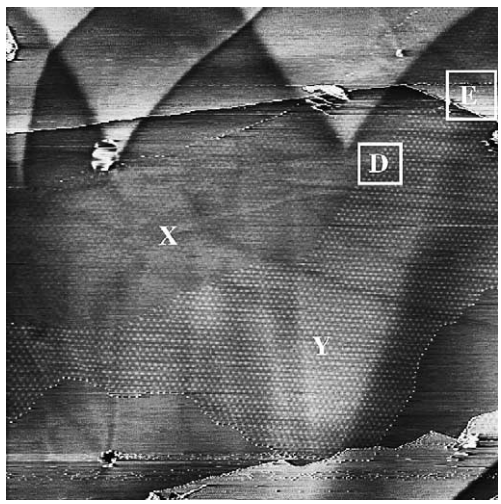

Fig. 1. Larger area STM image of the surface superlattice of graphite: two superlattice domains are marked as X and Y (640 nm × 640 nm, $V_{sample} = 0.1$ V, $I_t = 1.0$ nA).

D region in Fig. 1, is shown in Fig. 2(a) and (b). Two domains have the same periodicity, 80 Å. According to the rotation moiré pattern hypothesis, the rotation angle θ and the periodicity D is correlated by

$$D = \frac{d}{2 \times \sin\left(\frac{\theta}{2}\right)}, \tag{1}$$

where $d = 2.456$ Å is the lattice constant of graphite. For the measured value, 80 Å, the rotation angle is $\theta = 1.76°$. The orientation angle ϕ of the superlattice with respect to the atomic lattice of the top-layer is

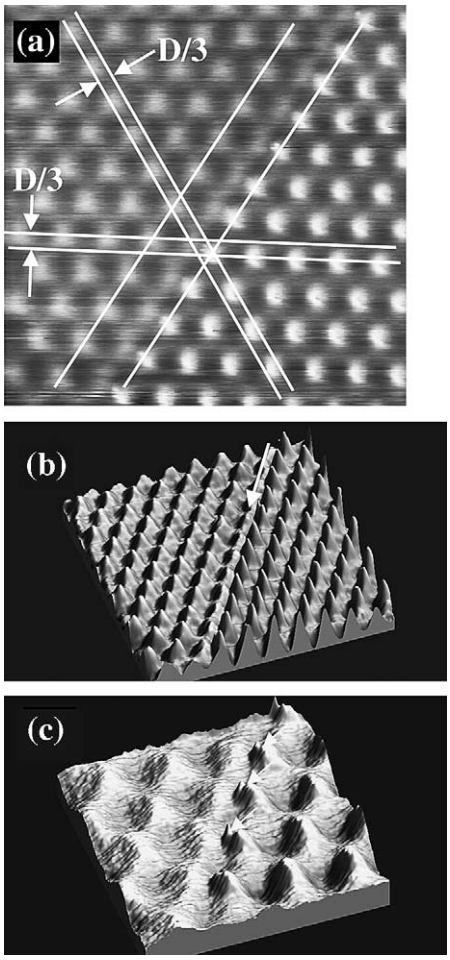

Fig. 2. (a) A close view of the moiré pattern domains in the D region of Fig. 1 (72 nm × 72 nm, $V_{sample} = 0.1$ V, $I_t = 1.0$ nA). (b) Three dimensional presentation of (a). (c) A closer view of the boundary in (b) (32 nm × 32 nm, $V_{sample} = 0.1$ V, $I_t = 1.0$ nA).

$$\phi = 30° - \frac{\theta}{2} \tag{2}$$

we obtain $\phi = 29.12°$.

The vertical corrugation is dramatically different for the X and Y regions, and the Y region exhibits much larger contrast, which can be more clearly observed in the 3D image (Fig. 2(b)). The averaged contrast for the X and Y regions are 1.7 and 3.8 Å, respectively. A row with the lowest vertical corrugation occurs at the boundary, as indicated by the arrow in Fig. 2(b). The superlattices in both X and Y domains remain a three-fold symmetry, which is an intrinsic characteristic of the rotation resulted moiré pattern. However, two of the three close-packing directions in the X domain are shifted about $D/3$ with respect to their counterparts in Y domain, as highlighted by the white lines in Fig. 2(a). A closer view of the boundary is shown in Fig. 2(c). In Fig. 2(c), we see some satellite peaks (marked by the arrows) next to the contrast maxima in the Y domain, which may be related to disruption of the graphite network in this high strained boundary region. We could easily obtain atomic resolution images in both X and Y domains, as shown in Fig. 3. The orientation angle ϕ is measured from Fig. 3 to be $29 \pm 2°$. However, tunneling become unstable at the boundary and no defined atomic resolution STM

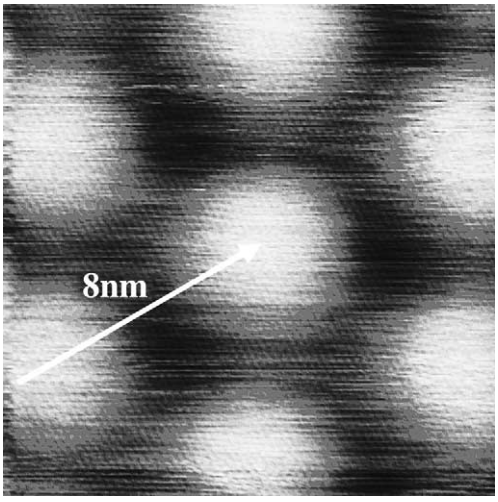

Fig. 3. Atomic resolution STM image of moiré pattern in the Y region.

images could be obtained. In spite of the poor resolution and sharp peaks in the boundary region, the top layer is still a consecutive carbon network without any prominent layer tearing. The smooth topography of Fig. 2(c) also dictates this case.

Now there are two points needed to be addressed: The first one is why the superlattices with the same periodicity have so different vertical contrasts, and the other is how the $D/3$ shift forms.

Fig. 4(a) shows an STM image recorded from the E region of Fig. 1. The superlattices of Y domain extend over the whole E region, and are divided into three parts, Y, F and G, by the dashed lines. The Y region is a direct moiré pattern, and the F and G regions are one layer higher. The observation suggests that the superlattices one layer below could be imaged. The averaged vertical corrugation for the Y region is 3.8 Å, and for the E and G regions it is about 1.6 Å. Therefore, the attenuation factor is 2.4 (3.8 Å/1.6 Å) per monolayer, which is very close to 2.6, reported by Rong [9]. As mentioned previously, the averaged corrugation in the X region is about 1.7 Å, which implies that the superlattice observed in the X region may be related to some subsurface feature.

Assuming that the moiré pattern in the X region is from subsurface, the stacking sequence in the X and Y regions will be very interesting. As the Y region has larger corrugation, what we see in the Y region is a direct moiré pattern. The direct moiré pattern results from a small angle rotation of the top layer, and thus the stacking sequence is A_RBAB, where the subscript R denotes a rotation of the A layer with respect to the normal stacking sequence ABAB in graphite. Because the X and Y domains have the same top layer, the subsurface moiré pattern formed in the X region should have a stacking sequence A_RB_RAB. In this case, two subsurface layers, B_RA, form the moiré pattern, and its vertical corrugation will be significantly attenuated by the top layer A_R, which explains why the X region has lower contrast.

The second layer in the X region is rotated by a small angle, θ, with respect to its counterpart in the Y region. This will make the boundary of the X and Y regions highly strained. The abrupt smaller peaks observed in Fig. 2(c) are probably associated with the displacements of carbon atoms in this highly strained area.

Next, we will show how the second-layer rotation could give rise to a $3/D$ shift as observed in Fig. 2(a). To simulate the STM images with this rotation, we use the model as proposed by Cee et al. [10]. The graphite layer is simulated by Formula (3), which is used to characterize a continuous hexagonal lattice similar to the carbon lattice of a graphite layer. The wave function density of the nth graphite layer, $\delta_n(x,y)$, at point (x,y) is given by

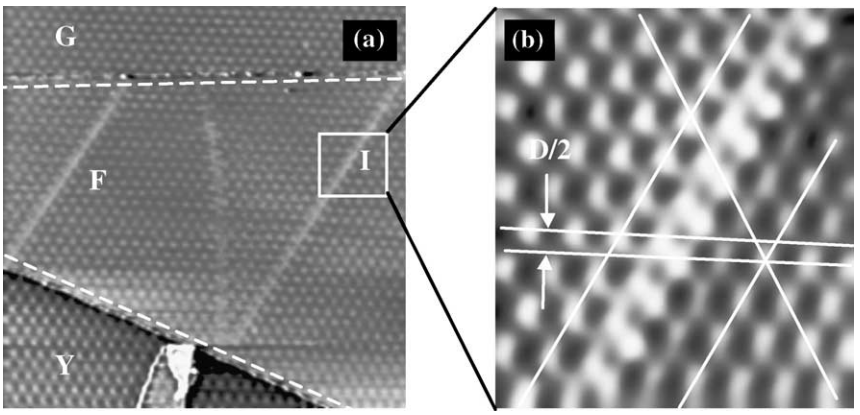

Fig. 4. (a) Superlattice in the E region of Fig. 1 (240 nm×240 nm, $V_{sample} = 0.1$ V, $I_t = 1.0$ nA). (b) Closer view of I region (a) (64 nm×64 nm, $V_{sample} = 0.1$ V, $I_t = 1.0$ nA).

$$\delta_n = 1 - \frac{2}{9}\left\{ \cos\left[\frac{2\pi}{2.46}\left(x' + \frac{y'}{\sqrt{3}}\right)\right] + \cos\left[\frac{2\pi}{2.46}\left(x' - \frac{y'}{\sqrt{3}}\right)\right] + \cos\left[\frac{4\pi}{2.46}\left(\frac{y'}{\sqrt{3}}\right)\right] + \frac{3}{2}\right\}, \quad (3)$$

where $x' = x^{\cos\theta} - y^{\sin\theta}$, $y' = x^{\sin\theta} + y^{\cos\theta}$, and θ is the rotation angle. At any point (x, y) of the top layer, STM image can be simulated by

$$I^2(x,y) = \delta_1(x,y) - b\delta_2(x,y) + c\delta_3(x,y), \quad (4)$$

where $\delta_n(x,y)$ is the density of the wave function for the nth layer at (x,y) position, and I^2 is the density of states seen by STM. Constants b and c determine the contributions from the second and third layer, respectively. As the inter-layer interaction in graphite is weak and the STM is only sensitive to the local density of states near the surface Fermi level, three layers are enough to simulate STM images. For $b = 0.5$ and $c = 0.125$ and a small rotation angle of the top layer, we can produce image that agrees very well with the STM image of the moiré pattern.

For the A_RB_RAB stacking in the X region and the A_RBAB stacking in the Y region, the simulation is straightforward. First, we use A_RBA three layers to construct a moiré pattern. Along one close-packed direction, the image is divided into two halves. One half remains unchanged, which gives the moiré pattern in the Y region. The other half is reset to the B_RAB stacking in the X region, and is recalculated to construct its moiré pattern. Here, the moiré pattern with the B_RAB stacking sequence is still a direct one. We do not want to discuss the overlayer attenuation effect using this model, which has been discussed in details previously [9]. In the calculation process, we find that the model is sufficient for the analysis of symmetry of a moiré pattern. To save the computer memory, we choose a rotation angle of 4°, which have no effect on the physical meaning of the results.

The simulated image is shown in Fig. 5. We draw lines along three close-packed directions. Two of them are shifted by $D/3$ and the other one remains parallel, which is in very good agreement with what observed in Fig. 2(a). Therefore, the

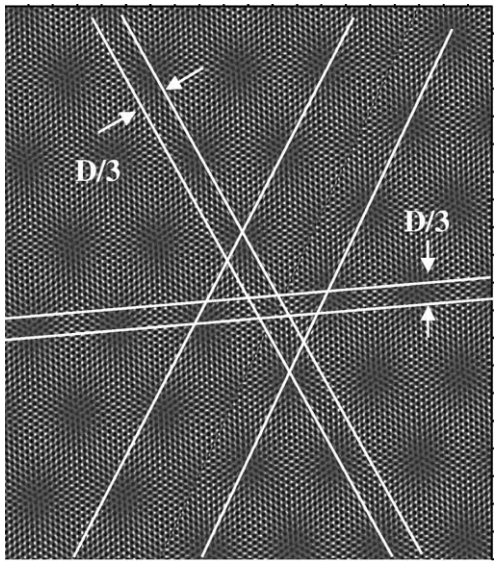

Fig. 5. Simulated STM image of the twist boundary (20 nm × 20 nm).

different vertical corrugation and symmetry in the X and Y regions are due to the double-layer rotation in the X region. The boundary between the X and Y regions is a twist boundary, which may be formed in the growth process or during cleavage.

In Fig. 4(a), two parallel rows of bright protrusions are observed. A closer view of the STM image taken from I region is shown in Fig. 4(b). We find that one close-packed direction is shifted by $D/2$, while the other two remain parallel. Therefore, it corresponds to another kind of moiré pattern domain boundary.

We expect that the shearing force exerted by exterior objects may cause a relative gliding of carbon atoms in the graphite layer and that the domain boundary observed in Fig. 4(b) is due to this gliding. Although gliding can take place along any directions, for simplicity of calculations, we only consider two cases: the gliding along the 30° or 60° direction as indicated by the arrows in Fig. 6. The gliding along the 30° direction has a periodicity of three times of the carbon bond length, i.e. 1.42 Å × 3 = 4.26 Å, while that along the 60° direction has a periodicity of 2.45 Å.

First, we use A_RBA sandwiched layers to form a moiré pattern. Along one close-packed direction

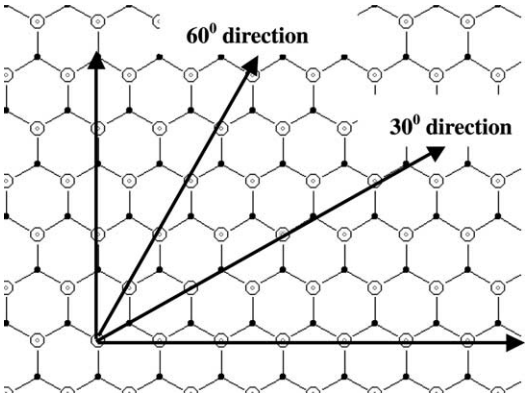

Fig. 6. Schematic drawing of the graphite lattice: the open and solid balls denote α- and β-sites, respectively.

the surface is divided into two halves. One half remains unchanged, which produce the normal moiré pattern with $A_R BA$ stacking. The top layer A_R of the other half makes a glide along the 30°/60° direction. The moiré pattern can recover when the gliding distance is integral times of the periodicity. However, with fractional periodicity, two halves of the moiré patterns have different symmetries with respect to each other.

For a gliding along 30° direction, the simulated moiré pattern with a gliding distance of one third of the periodicity, 1.42 Å, is shown in Fig. 7. We see that two of the three close-packed directions are shifted by about $D/3$. The simulated image in Fig. 7 is almost the same as Fig. 5. But the formation mechanism is so different; one is associated with rotation and the other with gliding. Therefore, it is insufficient to distinguish twisting from gliding only based on a symmetry consideration. Together with the vertical corrugation difference, we conclude that the boundary between the X and Y domains is not related to gliding.

For gliding along 60° direction, the simulated STM image with a gliding distance of half of the periodicity, 2.456 Å/2, is shown in Fig. 8. A shift of $D/2$ along one close-packed direction is immediately evident. The symmetry of the simulated image also agrees with the experiment in Fig. 4(b). For other gliding distances along 60° direction, the simulated images are different from the experimental data. Therefore, the domain boundary in

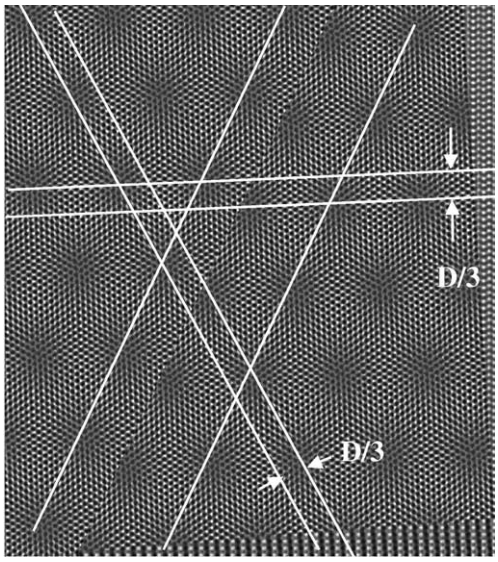

Fig. 7. Simulated STM image of the glide boundary along the 30° direction with a gliding distance of one third of the periodicity, 1.42 Å (20 nm × 20 nm).

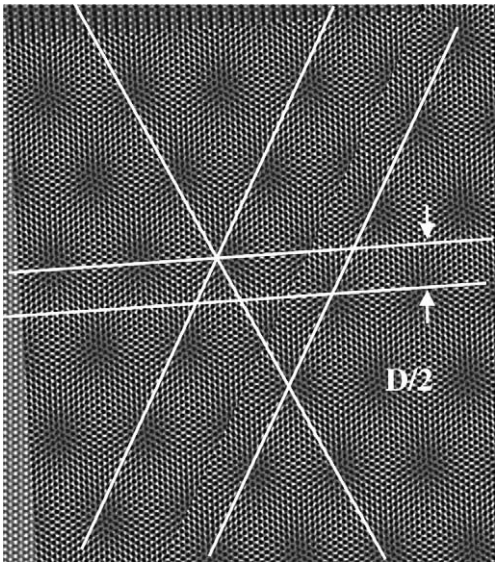

Fig. 8. Simulated STM image of the glide boundary along the 60° direction with a gliding distance of half of the periodicity, 2.456/2 Å (20 nm × 20 nm).

Fig. 4(b) is a result of gliding with a distance of 2.456 Å/2.

Based on the above simulations, the STM data could be well understood in the terms of

the rotational moiré pattern hypothesis. The shifts in different directions are formed by either intra-layer twisting or gliding. These kinds of motions of the carbon atoms in a graphite layer make the boundary region highly strained. The bright protrusion lines in Fig. 4(b) could be an indication of the enhanced local density of near the Fermi level under high strain.

4. Summary

Two types of domain boundaries of moiré patterns on the graphite surface are identified by STM observation and simulation. The first type is associated with intra-layer twisting and the second with intra-layer gliding. The intra-layer distortion may strengthen the inter-layer coupling, and thus have significant effect on the electronic structure of graphite.

Acknowledgements

This work is supported by National Science Foundation of China under contract nos. 60021403, 10134030 and F040503.

References

[1] R. Wiesendanger, Scanning Tunneling Microscopy and Spectroscopy: Methods and Applications, Cambridge University Press, Cambridge, 1994.
[2] D. Tomanek, S. Louie, Phys. Rev. B 37 (1988) 8327.
[3] Z.Y. Rong, P. Kuiper, Phys. Rev. B 48 (1993) 17427.
[4] C.R. Clemmer, T.P. Beebe Jr., Science 251 (1991) 640.
[5] H. Chang, A.J. Bard, Langmuir 7 (1991) 1143.
[6] M. Kuwabara, D.R. Clarke, D.A. Smith, Appl. Phys. Lett. 56 (1990) 2396.
[7] J. Garbarz, E. Lacaze, G. Faivre, S. Gauthier, M. Schott, Philos. Mag. A 65 (1992) 853.
[8] J. Xhie, K. Sattler, M. Ge, N. Venkateswaran, Phys. Rev. B 47 (1993) 15835.
[9] Z.Y. Rong, Phys. Rev. B 50 (1994) 1839.
[10] V.J. Cee, D.L. Patrick, T.P. Beebe Jr., Surf. Sci. 329 (1995) 141.
[11] T.M. Bernhardt, B. Kaiser, K. Rademann, Surf. Sci. 408 (1998) 86.
[12] J. Osing, I.V. Shvets, Surf. Sci. 417 (1998) 145.
[13] P.J. Ouseph, Phys. Rev. B 53 (1998) 9610.
[14] B. Feddes, I.I. Kravchenko, L.E. Seiberling, Scanning 20 (1998) 376.
[15] K. Miyake, K. Akutsu, T. Yamada, K. Hata, R. Morita, M. Yamashita, H. Shigekawa, Ultramicroscopy 73 (1998) 185.
[16] H. Beyer, M. Muller, Th. Schimmel, Appl. Phys. A 68 (1999) 163.
[17] P.J. Ouseph, Appl. Surf. Sci. 165 (2000) 38.
[18] K. Kobayashi, Phys. Rev. B 53 (1996) 11091.